Beamforming Design for Integrated Sensing, Computation Over-the-Air, and Communication in Internet of Robotic Things

Kai Dong, *Member, IEEE,* Sergiy A. Vorobyov, *Fellow, IEEE,*
Hao Yu, *Member, IEEE,* and Tarik Taleb, *Senior Member, IEEE*

***Abstract*—The integration of communication and radar systems could enhance the robustness of future communication systems to support advanced application demands, e.g., target sensing, data exchange, and parallel computation. In this paper, we investigate the beamforming design for Integrated Sensing, Computing, and Communication (ISCC) in the Internet of Robotic Things (IoRT) scenario. Specifically, we assume that each robot uploads its pre-processed sensing information to the Access Point (AP). Meanwhile, leveraging the additive features of the spatial wireless channels between robots and AP, Over-the-air Computation (AirComp) through multi-robot cooperation could bolster system performance, particularly in tasks like target localization through sensing. To get a full picture of the effects of antenna array structures and beampatterns on the ISCC system, we evaluate the performance by considering the shared and separated antenna structures, as well as the omnidirectional and directional beampatterns. Based on these setups, the non-convex optimization problems for the performance tradeoff between sensing and AirComp are formulated to minimize the Mean Squared Error (MSE) of AirComp and sensing. To efficiently solve these optimization problems, we designed the Gradient Descent Augmented Lagrangian (GDAL) algorithm, which involves dynamically adjusting the step sizes while updating the variables. Simulation results show that the separated antenna structure achieves a lower AirComp MSE than the shared antenna setup because it has more beam steering degrees of freedom. Moreover, the beampattern types have almost no effect on the AirComp MSE for the given antenna structure setup. This comprehensive investigation provides useful guidelines for ISCC framework implementation in IoRT applications.**

***Index Terms*—Beamforming, Over-the-air Computation, Integrated Sensing, Computation, and Communication, Internet of Robotic Things.**

I. Introduction

THE evolving wireless technology has been regarded as a pivotal facilitator for the future Internet of Robotic Things (IoRT), a specific use case of the Internet of Things (IoT) ecosystem, owing to its enhanced functionalities in connectivity, communication, and interaction [1]. Smart IoRT systems focus on integrating robotic systems into connected networks to meet a variety of service needs. For example, they collect real-time data from the environment using sensors (like radar sensors), process the data locally or remotely at the edge server, and send the data to other devices or centralized systems [2]. This poses new challenges for integrated framework design for IoRT systems, especially for mobile robots. The emerging integrated sensing and communication (ISAC) techniques provide a solution for simultaneous data collection via sensing sensors and data exchange via communication [3], [4]. Moreover, the enormous amount of sensing data generated in such systems forces us to design more efficient computation schemes, such as the computation function realized locally at the robot, at the nearby edge server, or over the air utilizing the analog-wave summation in the physical layer [5]. These considerations motivated us to develop a hybrid ISCC framework tailored to meet the demanding service requirements of IoRT.

The ISCC is crucial for IoRT systems to achieve real-time decision-making, efficient resource utilization, and robust fault tolerance. (*i*) ***Real-time decision making:*** The IoRT system operates in dynamic and uncertain environments where quick decision-making is of paramount importance. In the ISCC system framework, the robots can collect real-time data from their surroundings via sensing (e.g., radar), process it locally or collaboratively, and make autonomous decisions without relying solely on a centralized controller or human intervention [6]. (*ii*) ***Enhanced resource utilization efficiency:*** Integrated IoRT systems can enhance resource utilization efficiency by leveraging distributed sensing and computation. Specifically, instead of transmitting raw sensor data to a central processing unit (e.g., an edge server), robots can pre-process and analyze data locally to reduce data transmission and further minimize latency. Moreover, both radar sensing and data transmission using the same spectrum and signals can improve bandwidth and energy efficiencies, making IoRT systems more efficient and scalable for simultaneously serving multiple robots [7]. (*iii*) ***Robust error-fault tolerance:*** The IoRT system enables robots to collaborate with each other to achieve common goals or tasks. For example, when multiple robots send their collected sensing information about one common target to the edge server via multi-access wireless channels, the localization

This work was partially supported by the European Union's HE research and innovation program HORIZON-JUSNS-2023 under the 6G-Path project (Grant No. 101139172). The paper reflects only the authors' views, and the European Commission bears no responsibility for any utilization of the information contained herein.

Kai Dong is with the Center of Wireless Communications, University of Oulu, 90570 Oulu, Finland. (e-mail: kai.dong@oulu.fi)

Sergiy A. Vorobyov is with the Department of Information and Communications Engineering, Aalto University, 02150 Espoo, Finland (e-mail: sergiy.vorobyov@aalto.fi)

Hao Yu is with ICTFicial OY, 02130 Espoo, Finland. (*Corresponding Author*, e-mail: hao.yu@ictficial.com)

Tarik Taleb is with the Faculty of Electrical Engineering and Information Technology, Ruhr University Bochum, 44801 Bochum, Germany. (e-mail: tarik.taleb@rub.de)

parameter estimation leveraging the information from multiple robots could achieve an enhanced robustness for errors (faults) compared to a single robot [8].

The dual-functional waveform design becomes of paramount importance to meet various service quality requirements. The optimal waveform design with constraint of a fixed transmit power, for achieving the sensing and downlink communication performance tradeoff has been investigated in [9] where an ISAC system was mounted at the Base Station (BS). By fully using the waiting time in conventional pulsed radar to transmit dedicated communication signals, the waveform has been designed to improve the communication spectrum efficiency and probability of target detection in a full-duplex ISAC scheme [10]. From the perspective of information theory (Mutual Information (MI)), another waveform has been designed to maximize the sensing and communication MI [11]. To detect the target behind the obstacle, the Reconfigurable Intelligent Surface (RIS) has also been utilized to assist the downlink simultaneous target sensing and communication via beamforming design [12]. In [13], Unmanned Aerial Vehicles (UAVs) has been designed to provide ISAC services for multiple IoT nodes to maximize the minimum data rate. Although the aforementioned works focus on the ISAC waveform design to enhance the Quality of service (QoS), the antenna configuration types (shared or separated antenna array structures) and the beampattern types (omnidirectional or directional) are not explored for the ISAC system design, which is crucial from the perspective of ISCC framework design for meeting various QoS requirements [14].

In mobile IoRT systems, the robots need to continuously perform sensing for environment perception, object detection (e.g., obstacles and landmarks), and localization [2]. There will be enormous amounts of raw data collected at the sensors. Therefore, related data processing (computation) is necessary. However, the limited battery at the mobile robot forces us to design energy-efficient computation schemes, e.g., the hybrid local data pre-processing at the IoT device plus the post-processing at the edge server [15]–[18]. Thus, the pre-processed sensing data is offloaded to the edge server for data post-processing via the multi-access wireless channels between robots and BS, or AP, for computation efficiency enhancement and energy conservation. Furthermore, AirComp fully utilizing the additive properties of analog signals via multi-access wireless channels through multi-IoT device co-operation has been proposed as a promising method for fast data aggregation at the centralized receiver (e.g., BS or AP) in the physical layer [19]–[22]. Therefore, the integration of AirComp with ISAC technology, i.e., the ISCC framework, has many advantages, such as improved spectrum efficiency using the same spectrum resources and enhanced QoS performance through multi-device cooperation (e.g., target localization), etc. [7], [20], [23]–[25]. In [7], the radar and communication signals transmitted through shared or separated antenna arrays have been considered for wireless sensor networks. The beamforming design has been optimized to minimize AirComp errors. The beampattern has been designed in [26] to achieve a performance tradeoff between sensing and AirComp

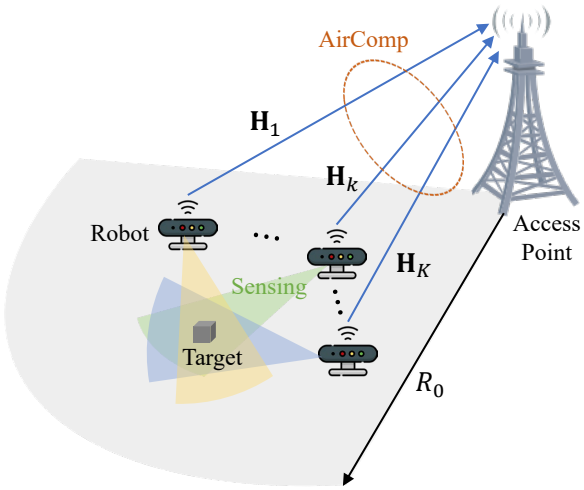

Fig. 1: ISCC framework implemented in an IoRT scenario.

constrained by the power budget at each device. In particular, omnidirectional and directional beampatterns were considered. Similarly, the performance tradeoff among communication, sensing, and computation under power constraints has been investigated in [24]. The authors of [20] designed beamforming for sending a superposition-coded signal to the BS over the uplink channel for computation and communication. The minimum communication data rate and power constraints have been considered when determining the optimal beamforming matrix. However, the aforementioned literature does not have a comprehensive analysis of the antenna array structures (shared or separated) and the beampatterns (omnidirectional or directional). Furthermore, these works evaluate the system performance using a random Gaussian channel realization rather than considering practical path loss in high-frequency bands or link conditions such as blockage. Those realistic setups will be considered in this paper in the IoRT scenario, as depicted in Fig. 1.

The specific contributions of this paper are as below:

- In addition to the shared and separated antenna array structures at each robot for both communication and sensing, we also take into account the omnidirectional and directional beampatterns to conduct a comprehensive comparison between these near-realistic setups in an IoRT scenario.
- To achieve a performance tradeoff between sensing and AirComp, several non-convex MSE minimization-based optimization problems are formulated under the constraints of maximum transmit power and sensing QoS requirements for different antenna array setups and beampatterns.
- To solve these non-convex optimization problems efficiently, we designed a GDAL algorithm with adaptive adjustment of the step size when updating the variable using gradient descent method.
- The propagation of electromagnetic wave signals between the robot and AP is prone to being blocked in the high-frequency bands. Here, we also explore the AirComp

MSE affected by the robot-AP link blockage that happened with a certain probability.

The rest of this paper is organized as follows: Section-II introduces the system models for two different antenna structures at robots. The optimal beampattern design for radar sensing is described in Section III. Section IV introduces the optimization problem and gives corresponding algorithm for the performance tradeoff optimization between sensing and AirComp. Numerical simulation results and conclusion remarks are presented in Sections V and VI, respectively.

Notations: In this paper, we use bold lowercase letters (e.g., $\mathbf{a}$) and bold uppercase letters (e.g., $\mathbf{A}$) to represent vectors and matrices, respectively. By normal fonts (e.g., a), we denote the scalars. Moreover, $\mathbf{Tr}(\cdot)$ stands for the trace operation, $(\cdot)^H$ denotes the Hermitian transpose operation, $\|\cdot\|_F$ represents the Frobenius norm of a matrix, $|\cdot|$ is the absolute value, and $\mathbf{I}$ is the identity matrix.

II. System Model

Consider a scenario with K robots randomly distributed at the sector coverage area of an AP with a radius of R_0, as illustrated in Fig. 1. There is a common point-like static target located at $[x_0, y_0]$. Accurate parameter estimation (e.g., coordinates and angle) of the target becomes of paramount importance for safety operation at the robot itself, or for end-to-end wireless link quality guarantees for the robot through proper propagation path scheduling. In this IoRT scenario with an ISCC framework, each robot simultaneously transmits the signals for target sensing and data transmission to the AP for AirComp. Assuming that the data symbols sent from each robot to the AP convey the estimated position information about the target in the last time slot, the AirComp using multi-robot cooperation could improve the target localization accuracy [7]. This is crucial for centralized resource management on the whole IoRT scenario.

The robots and AP are assumed to be equipped with Uniform Linear Arrays (ULAs) of N_R and N_A antenna elements, respectively. In particular, the N_t antenna elements out of the N_R ones at each robot are used for signal transmission, and the other $N_r = N_R - N_t$ ones are used for signal reception. The channel between the AP and each robot $k \in \mathcal{K} = \{1, 2, \cdots, K\}$ is assumed to be block-fading and the channel state information (CSI) is assumed to be accurately known at the AP. In mobile robotic networks operating in high-frequency bands, the electromagnetic wave signal propagation between AP and robots is prone to being blocked by the surrounding environment.[1] Here, we assume that the propagation link between AP and each robot is in a Line-of-sight (LoS) condition with probability $1 - p_b$ where $p_b \in [0, 1]$ denotes the blockage probability, and the pathloss is calculated according to Third Generation Partnership Project (3GPP) [29].

The received signal model at the AP depends on the antenna configurations of the robots, i.e., the sensing signals and the communication symbols can be either jointly transmitted using one shared transmitting antenna array via a dual-functional waveform or separately sent via two isolated ULAs. Both options will be presented in the following subsections.

A. Shared Antenna Configuration

In the shared antenna configuration, all the N_t transmitting antenna elements at each robot are used for both target sensing and data transmission to the AP, and the other N_r antennas are used for signal reception. The data symbols transmitted by the k-th robot for AirComp are expressed as $\mathbf{s}_k[t] = \{g_{k,1}(\cdot), g_{k,2}(\cdot), \cdots, g_{k,M}(\cdot)\} \in \mathbb{C}^{M\times 1}$ where M is the number of functions to be computed [20], and $g_{k,m}(\cdot)$ represents the pre-processing function at the k-th robot. We assume the transmitted data symbols to be independent and identically distributed (i.i.d.), with zero mean and unit variance, i.e., $\mathbb{E}[\mathbf{s}_k[t]\mathbf{s}_k[t]^H] = \mathbf{I}_M$ and $\mathbb{E}[\mathbf{s}_k[t]\mathbf{s}_\varrho[t]^H] = \mathbf{0}, \forall\, k \neq \varrho$. Then the transmitted signal can be written as

$$\mathbf{x}_k[t] = \mathbf{F}_k \mathbf{s}_k[t] \tag{1}$$

where $\mathbf{F}_k \in \mathbb{C}^{N_t\times M}$ denotes the beamforming precoder implemented at the k-th robot. Generally, the signals reflected by the target are vanished at the AP due to the long distance between the robot and AP. Thus, the received signal vector with the beamforming combiner $\mathbf{W} \in \mathbb{C}^{N_A\times M}$ at the AP can be formulated as

$$\mathbf{y}[t] = \sum_{k=1}^{K} \mathbf{W}^H \mathbf{H}_k \mathbf{F}_k \mathbf{s}_k[t] + \mathbf{W}^H \mathbf{n} \tag{2}$$

where $\mathbf{H}_k \in \mathbb{C}^{N_A\times N_t}$ denotes the Multiple Input Multiple Output (MIMO) channel between the k-th robot and AP, and $\mathbf{n} \in \mathbb{C}^{N_A\times 1}$ is the AWGN noise vector such that $\mathbf{n} \sim \mathcal{CN}(\mathbf{0}, \sigma_n^2\mathbf{I})$. Limited by the power budget $P_{\max}$ for the precoder design at each robot, we should meet the following constraint:

$$\|\mathbf{F}_k\|_F^2 \leq P_{\max}\ . \tag{3}$$

Assuming that the channel matrix $\mathbf{H}_k$ between AP and each robot is known at the AP,[2] the ideal received signal $\tilde{\mathbf{y}}[t]$ (i.e., no link blockage and with optimal beamforming design) is given by

$$\tilde{\mathbf{y}}[t] = \sqrt{\frac{P_t}{M}} \sum_{k=1}^{K} \mathbf{U}^H \mathbf{H}_k \mathbf{V}_k \mathbf{s}_k[t] \tag{4}$$

where $P_t \leq P_{\max}$ denotes the transmit power at the robot for both sensing and AirComp signal transmission via the dual-functional waveform, $\mathbf{V}_k \in \mathbb{C}^{N_t\times M}$ contains the first M right singular vectors in the Singular Value Decomposition (SVD) of $\mathbf{H}_k$, i.e., the optimal beamforming precoders for implementation, $\mathbf{U} \in \mathbb{C}^{N_A\times M}$ collects the first M left singular vectors of the SVD of $\sum_{k=1}^{K} \mathbf{H}_k$, i.e., the designed aggregation beamforming combiner at AP for receiving the signals from all the K robots. Note that the beamforming design steered to the dominant signal reception directions based on SVD of the MIMO channel by exploiting channel sparsity has been widely

[1] The blockage effect can be mitigated by emerging relaying technologies such as smart repeaters and reconfigurable metasurfaces, refer to [27], [28] for more details.

[2] For related channel estimation methods refer to [30], [31].

utilized for maximizing the received signal power [32], [33]. Thereby, we derive the aforementioned optimal precoders at each robot based on the channel between the robot and AP, and the optimal aggregation combiners at AP according to the summation of all the channels between robots and AP. Then we can get the ideal received signal in (9) and regard it as a benchmark for MSE computation of the received signal (2) as:

$$\begin{aligned}\mathbf{MSE}_{\text{AirComp}} &= \mathbb{E}_t\left[|\mathbf{y}[t]-\tilde{\mathbf{y}}[t]|^2\right] \\ &= \sum_{k=1}^{K}\|\mathbf{W}^H\mathbf{H}_k\mathbf{F}_k-\mathbf{A}\|_F^2+\sigma_n^2\|\mathbf{W}\|_F^2 \quad (5)\end{aligned}$$

where $\mathbf{A}\triangleq\sqrt{\frac{P_t}{M}}\mathbf{U}^H\mathbf{H}_k\mathbf{V}_k$.

B. Separated Antenna Configuration

Unlike the shared antenna configuration for both sensing and communication via the dual-functional waveform at each robot, the transmitting antennas are split into two sub-ULA arrays ($N_t = N_s + N_c$) in the separated antenna structure. Here, N_s antenna elements are used for radar sensing and N_c antenna elements are used for data transmission to the AP. The sensing symbols at the k-th robot can be denoted as $\mathbf{d}_k[t]\in\mathbb{C}^{\bar{M}\times 1}$ where $\bar{M}$ represents the number of beams for radar sensing ($\bar{M}\geq 1$), and $\mathbb{E}[\mathbf{d}_k[t]\mathbf{d}_k[t]^H]=\mathbf{I}_{\bar{M}}$ and $\mathbb{E}[\mathbf{d}_k[t]\mathbf{d}_t[t]^H]=\mathbf{0},\forall\, k\neq\varrho$. Similar to the shared antenna configuration, the data symbols uploaded to the AP for AirComp are expressed as $\mathbf{s}_k[t]\in\mathbb{C}^{M\times 1}$ where M is the number of functions to be computed. Then the transmitted signals from each robot can be written as

$$\mathbf{x}_k[t]=\begin{bmatrix}\bar{\mathbf{F}}_k\mathbf{d}_k[t]\\ \mathbf{F}_k\mathbf{s}_k[t]\end{bmatrix} \quad (6)$$

where $\mathbf{F}_k\in\mathbb{C}^{N_c\times M}$ and $\bar{\mathbf{F}}_k\in\mathbb{C}^{N_s\times\bar{M}}$ are the beamformers for data transmission and radar sensing, respectively. Ignoring the signals reflected from the target to the AP, due to the large distance, the received aggregated symbol vector $\mathbf{y}[t]$ at the AP can be expressed as

$$\mathbf{y}[t]=\sum_{k=1}^{K}\left(\mathbf{W}^H\mathbf{H}_k\mathbf{F}_k\mathbf{s}_k[t]+\mathbf{W}^H\bar{\mathbf{H}}_k\bar{\mathbf{F}}_k\mathbf{d}_k[t]\right)+\mathbf{W}^H\mathbf{n} \quad (7)$$

where $\bar{\mathbf{H}}_k\in\mathbb{C}^{N_A\times N_s}$ and $\mathbf{H}_k\in\mathbb{C}^{N_A\times N_c}$ represent the MIMO channels between AP and the k-th robot for sensing signals and data transmission, respectively, and $\mathbf{n}\in\mathbb{C}^{N_A\times 1}$ is the i.i.d. noise vector such that $\mathbf{n}\sim\mathcal{CN}(\mathbf{0},\sigma_n^2\mathbf{I})$.

Similar to the shared antenna configuration, both designed transmitting precoders $\bar{\mathbf{F}}_k$ and $\mathbf{F}_k$ should meet the maximal transmit power constraint that takes the following form:

$$\|\bar{\mathbf{F}}_k\|_F^2+\|\mathbf{F}_k\|_F^2\leq P_{\max}\ . \quad (8)$$

Similar to the signal model of the shared antenna structure, the ideal received signal $\tilde{\mathbf{y}}[t]$ (given the knowledge about channel $\mathbf{H}_k$ between AP and each robot) can be expressed as

$$\tilde{\mathbf{y}}[t]=\sqrt{\frac{P_t}{M}}\sum_{k=1}^{K}\mathbf{U}^H\mathbf{H}_k\mathbf{V}_k\mathbf{s}_k[t] \quad (9)$$

where $P_t\leq P_{\max}$ is the transmit power for AirComp, $\mathbf{V}_k\in\mathbb{C}^{N_s\times M}$ and $\mathbf{U}\in\mathbb{C}^{N_A\times M}$ have the same expressions as in (9).

The corresponding MSE between the received signal (7) and the ideal one $\tilde{\mathbf{y}}[t]$ in (9) is given by

$$\begin{aligned}\mathbf{MSE}_{\text{AirComp}} &= \mathbb{E}_t\left[|\mathbf{y}[t]-\tilde{\mathbf{y}}[t]|^2\right] \\ &= \sum_{k=1}^{K}\|\mathbf{W}^H\mathbf{H}_k\mathbf{F}_k-\mathbf{A}\|_F^2 \\ &\quad+\sum_{k=1}^{K}\|\mathbf{W}^H\bar{\mathbf{H}}_k\bar{\mathbf{F}}_k\|_F^2+\sigma_n^2\|\mathbf{W}\|_F^2\ . \quad (10)\end{aligned}$$

III. BeamPattern Design

According to the knowledge level about the target, the beampattern design can be divided into two types: omnidirectional and directional beampatterns. The former design is suitable for the blinding sensing stage, where there is a lack of knowledge about the target direction. It is the case for example during the initial target sensing stage. On the other hand, the second design is specifically targeted for situations where the sensing directions are known and the target is being tracked. Corresponding beampattern designs are introduced next.

A. Omnidirectional Beampattern Design

For the omnidirectional beampattern, the beamforming matrix $\mathbf{F}_k$ should be orthogonal with an identity covariance matrix [9]. To minimize the AirComp errors defined in (5) and (10), the following optimization problems are formulated for two different antenna configurations that are stated in Section-II. For shared antenna configuration:

$$\begin{aligned}\mathbf{P1.1}\quad &\min_{\mathbf{F},\mathbf{W}}\quad \boldsymbol{\mathcal{F}}_{1.1}\left(\mathbf{F}_k,\mathbf{W}\right) \\ &\qquad=\sum_{k=1}^{K}\|\mathbf{W}^H\mathbf{H}_k\mathbf{F}_k-\mathbf{A}\|_F^2+\sigma_n^2\|\mathbf{W}\|_F^2 \quad (11a)\\ &\quad s.t.\quad \|\mathbf{F}_k\|_F^2=P_{\max},\,\forall k \quad (11b)\end{aligned}$$

and for separated antenna configuration:

$$\begin{aligned}\mathbf{P2.1}\quad &\min_{\mathbf{F},\mathbf{W},\bar{\mathbf{F}}}\quad \boldsymbol{\mathcal{F}}_{2.1}\left(\mathbf{F}_k,\mathbf{W},\bar{\mathbf{F}}_k\right) \\ &\qquad=\sum_{k=1}^{K}\|\mathbf{W}^H\mathbf{H}_k\mathbf{F}_k-\mathbf{A}\|_F^2 \\ &\qquad\quad+\sum_{k=1}^{K}\|\mathbf{W}^H\bar{\mathbf{H}}_k\bar{\mathbf{F}}_k\|_F^2+\sigma_n^2\|\mathbf{W}\|_F^2 \quad (12a)\\ &\quad s.t.\quad \|\mathbf{F}_k\|_F^2+\|\bar{\mathbf{F}}_k\|_F^2=P_{\max},\,\forall k\ . \quad (12b)\end{aligned}$$

Note that those two problems are non-convex due to the quadratic power constraints in (11b) and (12b). Although an Alternating Optimization (AO) approach can be utilized to solve problem $\mathbf{P1.1}$ as described in [26], the joint optimization of $\mathbf{F}=\{\mathbf{F}_1,\cdots,\mathbf{F}_k,\cdots,\mathbf{F}_K\}$ and $\bar{\mathbf{F}}=\{\bar{\mathbf{F}}_1,\cdots,\bar{\mathbf{F}}_k,\cdots,\bar{\mathbf{F}}_K\}$ makes it an inefficient approach for solving problem $\mathbf{P2.1}$. Here, we design a Gradient Descent Augmented Lagrangian (GDAL) algorithm. In particular, the

$$\mathcal{L}_{P1.2}(\mathbf{F}_k, \mathbf{W}, \bar{\mathbf{F}}_k, \lambda_k, \rho) = \boldsymbol{\mathcal{F}}_{1.2}\left(\mathbf{F}_k, \mathbf{W}, \bar{\mathbf{F}}_k\right) + \sum_{k=1}^{K} \lambda_k \left(\|\mathbf{F}_k\|_F^2 + \|\bar{\mathbf{F}}_k\|_F^2 - P_{\max}\right) + \frac{\rho}{2} \sum_{k=1}^{K} \left(\|\mathbf{F}_k\|_F^2 + \|\bar{\mathbf{F}}_k\|_F^2 - P_{\max}\right)^2 . \tag{13}$$

gradient descent approach is utilized to update the desired variables $\mathbf{F}_k, \bar{\mathbf{F}}_k$ and $\mathbf{W}$ based on the augmented Lagrangian function. In the following, the detailed procedures using the proposed GDAL approach for solving problem $\mathbf{P2.1}$ are presented.[3]

First, the augmented Lagrangian function for problem $\mathbf{P2.1}$ is defined in (13) at the top of this page, where λ_k denotes the Lagrange multiplier and the ρ represents the penalty parameter. After initializing the required parameters, we calculate the gradients with respect to $\mathbf{F}_k, \mathbf{W}$, and $\bar{\mathbf{F}}_k$ at each iteration as follows:

$$\nabla_{\mathbf{W}} \mathcal{L}_{P2.1} = 2 \sum_{k=1}^{K} \mathbf{H}_k \mathbf{F}_k \left(\mathbf{W}^H \mathbf{H}_k \mathbf{F}_k - \mathbf{A}\right) 2 \sum_{k=1}^{K} \bar{\mathbf{H}}_k^H \bar{\mathbf{F}}_k \mathbf{W}^H \bar{\mathbf{H}}_k \bar{\mathbf{F}}_k + 2\sigma_n^2 \mathbf{W} \tag{14}$$

$$\nabla_{\mathbf{F}_k} \mathcal{L}_{P2.1} = 2\mathbf{H}_k^H \mathbf{W} \left(\mathbf{W}^H \mathbf{H}_k \mathbf{F}_k - \mathbf{A}\right) + 2\lambda_k \mathbf{F}_k + 2\rho \left(\|\mathbf{F}_k\|_F^2 + \|\bar{\mathbf{F}}_k\|_F^2 - P_{\max}\right) \tag{15}$$

$$\nabla_{\bar{\mathbf{F}}_k} \mathcal{L}_{P2.1} = 2\bar{\mathbf{H}}_k^H \mathbf{W} \left(\mathbf{W}^H \bar{\mathbf{H}}_k \bar{\mathbf{F}}_k - \mathbf{A}\right) + 2\lambda_k \bar{\mathbf{F}}_k + 2\rho \left(\|\mathbf{F}_k\|_F^2 + \|\bar{\mathbf{F}}_k\|_F^2 - P_{\max}\right) . \tag{16}$$

Then the optimization variables at the l-th iteration can be updated as

$$\mathbf{W}^{l+1} = \mathbf{W}^l - \boldsymbol{\Phi}_{\mathbf{W}}^l \nabla_{\mathbf{W}} \mathcal{L}_{P2.1} \tag{17}$$

$$\mathbf{F}_k^{l+1} = \mathbf{F}_k^l - \boldsymbol{\Phi}_{\mathbf{F}_k}^l \nabla_{\mathbf{F}_k} \mathcal{L}_{P2.1} \tag{18}$$

$$\bar{\mathbf{F}}_k^{l+1} = \bar{\mathbf{F}}_k^l - \boldsymbol{\Phi}_{\bar{\mathbf{F}}_k}^l \nabla_{\bar{\mathbf{F}}_k} \mathcal{L}_{P2.1} . \tag{19}$$

The step sizes $\boldsymbol{\Phi}_{\mathbf{W}}$, $\boldsymbol{\Phi}_{\mathbf{F}_k}$, and $\boldsymbol{\Phi}_{\bar{\mathbf{F}}_k}$ can also be adaptively updated using the Adaptive Gradient Algorithm (AdaGrad) [34]–[36] based on the historical gradients to accelerate the convergence process compared to fixed step size method. This allows for larger step sizes in directions where the gradient is steep, facilitating faster progress towards the optimum, while smaller step sizes are employed in directions with less steep gradients. Here, we use a general expression to update each element (i-th row and j-th column) inside the step size $\boldsymbol{\Phi}$ for $\boldsymbol{\Phi}_{\mathbf{W}}$, $\boldsymbol{\Phi}_{\mathbf{F}_k}$, and $\boldsymbol{\Phi}_{\bar{\mathbf{F}}_k}$

$$[\boldsymbol{\Phi}^{l+1}]_{i,j} = \frac{[\boldsymbol{\Phi}^l]_{i,j}}{\sqrt{[\mathbf{G}^l]_{i,j}} + \zeta} \tag{20}$$

where ζ is a small positive scalar added to avoid division by zero, and the $[\mathbf{G}^l]_{i,j}$ records the sum of squared partial derivative for each element (i-th row and j-th column) of the corresponding variables accumulated over iterations. By implementation of (20), we can dynamically adjusting the step size for individual dimensions within the search space of each variable.

In the next step, the Lagrange multiplier λ_k and penalty parameter ρ are updated as

$$\lambda_k^{l+1} = \lambda_k^l + \rho \left(\|\mathbf{F}_k^l\|_F^2 + \|\bar{\mathbf{F}}_k^l\|_F^2 - P_{\max}\right) \tag{21}$$

$$\rho^{l+1} = \begin{cases} \min(\xi\rho^l, \rho_{\max}), & \delta^l \geq \delta_{th} \\ \max(\frac{\rho^l}{\xi}, \rho_{\min}), & \delta^l < \delta'_{th} \\ \rho^l, & \text{otherwise} \end{cases} \tag{22}$$

where δ^l indicates the constraint violation between $\|\mathbf{F}_k^l\|_F^2 + \|\bar{\mathbf{F}}_k^l\|_F^2$ and $P_{\max}$, ξ is a scaling factor (e.g., 2) and $\rho_{\max}$ is a maximum value for ρ^{l+1} to prevent it from growing too large. In particular, ρ^{l+1} will be increased if the violation is significant, i.e., $\delta^l \geq \delta_{th}$; otherwise, ρ^{l+1} will be decreased if the violation δ^l is minor, i.e., $\delta^l < \delta'_{th}$. A minimum constraint $\rho_{\min}$ is considered to prevent ρ^{l+1} from becoming too small.

The GDAL algorithm is stopped once the bias of the value of the Lagrangian function is not greater than the tolerance ϵ or the maximum number of iterations L is reached. The detailed procedures of GDAL algorithm are summarized in **Algorithm 1**. Thus, the optimal sensing precoder matrix $\mathbf{F}_k^*$ for each robot is derived, which will be used for the precoder and combiner design to achieve a performance tradeoff optimization in the next section.

B. Directional Beampattern Design

For the directional radar beampattern design, the directions of interest are specified in advance to design the covariance matrix $\mathbf{R}_k = \mathbf{F}_k \mathbf{F}_k^H \in \mathbb{C}^{N_t \times N_t}$ (Hermitian positive definite matrix). Given the angle directions of interest, the covariance matrix $\mathbf{R}_k$ design can refer to the procedures stated in [37], [38]

$$\min_{\mathbf{F}_k} \quad \left|\mathbf{g}(\theta) - \mathbf{a}(\theta)^H \mathbf{F}_k \mathbf{F}_k^H \mathbf{a}(\theta)\right| \tag{23a}$$

$$s.t. \quad \|\mathbf{F}_k\|_F^2 = P_t, \forall k \tag{23b}$$

where $\mathbf{a}(\theta) \in \mathbb{C}^{N_t \times 1}$ represents the steering vector in the direction of $\theta \in [-\pi/2, \pi/2]$ at the ULA of N_t transmitting antenna elements [27], $\mathbf{g}(\theta)$ denotes the desired beampattern [37], and $P_t \leq P_{\max}$ is the transmit power for radar sensing.[4]

[3]The procedure for solving problem $\mathbf{P1.1}$ follows similar steps, and thus, it is not presented here for the sake of brevity.

[4]This problem can be easily solved using the cvx toolbox [39], [40], more detailed discussion is out of the scope of this paper.

Algorithm 1: GDAL algorithm for Problem $\mathbf{P2.1}$

Input: Initialize $\mathbf{W}^0$, $\mathbf{F}^0$, $\bar{\mathbf{F}}^0$, λ^0, ρ^0, tolerance ϵ, step sizes $\mathbf{\Phi}_{\mathbf{F}_k}^0$, $\mathbf{\Phi}_{\mathbf{W}}^0$ and $\mathbf{\Phi}_{\bar{\mathbf{F}}_k}^0$, maximum number of iterations L.

Output: Optimal $\mathbf{F}$, $\mathbf{W}$ and $\bar{\mathbf{F}}$

$l \leftarrow 0$;
while $l < L$ **do**
  Sequentially update the parameters:
  Compute the value of the Lagrangian function in (13) ;
  Compute gradients of augmented Lagrangian function with respect to $\bar{\mathbf{F}}_k$, $\mathbf{F}_k$ and $\mathbf{W}$ defined in (14) - (16) ;
  Update $\bar{\mathbf{F}}_k$, $\mathbf{F}_k$ and $\mathbf{W}$ using gradient descent approach according to (17) - (19) ;
  Adaptively update the step sizes according to (20) ;
  Update λ_k^{l+1} according to (21) ;
  Update ρ^{l+1} defined in (22) ;
  Check convergence criteria:
  if *convergence criteria met* **then**
    Output $\mathbf{F}$, $\mathbf{W}$ and $\bar{\mathbf{F}}$;
    break ;
  $l \leftarrow l + 1$;

Similar to the omnidirectional beampattern design, the MSE minimization problems about AirComp can be formulated as

$$\mathbf{P3.1} \quad \min_{\mathbf{F},\mathbf{W}} \quad \boldsymbol{\mathcal{F}}_{3.1}\left(\mathbf{F}_k, \mathbf{W}\right) = \sum_{k=1}^{K} \|\mathbf{W}^H \mathbf{H}_k \mathbf{F}_k - \mathbf{A}\|_F^2 + \sigma_n^2 \|\mathbf{W}\|_F^2 \tag{24a}$$

$$s.t. \quad \mathbf{F}_k \mathbf{F}_k^H = \mathbf{R}_k, \, \forall k \tag{24b}$$

and

$$\mathbf{P4.1} \quad \min_{\mathbf{F},\mathbf{W},\bar{\mathbf{F}}} \quad \boldsymbol{\mathcal{F}}_{4.1}\left(\mathbf{F}_k, \mathbf{W}, \bar{\mathbf{F}}_k\right) = \sum_{k=1}^{K} \|\mathbf{W}^H \mathbf{H}_k \mathbf{F}_k - \mathbf{A}\|_F^2 + \sum_{k=1}^{K} \|\mathbf{W}^H \bar{\mathbf{H}}_k \bar{\mathbf{F}}_k\|_F^2 + \sigma_n^2 \|\mathbf{W}\|_F^2 \tag{25a}$$

$$s.t. \quad \bar{\mathbf{F}}_k \bar{\mathbf{F}}_k^H = \mathbf{R}_k \tag{25b}$$

$$\|\mathbf{F}_k\|_F^2 + \|\bar{\mathbf{F}}_k\|_F^2 = P_{\max}, \, \forall k \, . \tag{25c}$$

for shared antenna configuration setup and separated antenna setup, respectively.

Similar to problems $\mathbf{P1.1}$ and $\mathbf{P2.1}$, both $\mathbf{P3.1}$ and $\mathbf{P4.1}$ are non-convex, and they can also be solved by the proposed GDAL algorithm presented in **Algorithm 1**. First, we define the augmented Lagrangian functions for $\mathbf{P3.1}$ and $\mathbf{P4.1}$ in (26) and (27) shown at the top of this page, respectively. Then the problems can be solved by following the similar procedures described in **Algorithm 1**.[5]

IV. Beamforming Design for Performance tradeoff Optimization

In addition to the shared and separated antenna configurations presented in Section II, two beampatterns (omnidirectional and directional) for sensing are also considered here. Therefore, there are four different combinations of beampattrn schemes, as suggested by the optimal beampattern design problems of $\mathbf{P1.1}$ - $\mathbf{P4.1}$, which are formulated in Section-III. In this section, we consider the performance tradeoff optimization problems between AirComp and sensing given a weighting factor $\alpha \in [0, 1]$ and the optimal beampatterns $\mathbf{F}^* = \{\mathbf{F}_1^*, \cdots, \mathbf{F}_K^*\}$ that obtained from $\mathbf{P1.1}$ - $\mathbf{P4.1}$.

A. Problem Formulation with Performance tradeoff Optimization

After deriving the optimal beamformer $\mathbf{F}_k^*$ for each robot $\forall k$, the performance tradeoff optimization problems for all robots, by considering the total power constraint and sensing QoS requirement, can be reformulated as

$$\mathbf{P1.2} \quad \min_{\mathbf{F},\mathbf{W}} \quad \alpha \boldsymbol{\mathcal{F}}_{1.1}\left(\mathbf{F}_k, \mathbf{W}\right) + (1-\alpha) \sum_{k=1}^{K} \|\mathbf{F}_k - \mathbf{F}_k^*\|_F^2 \tag{28a}$$

$$s.t. \quad \|\mathbf{F}_k\|_F^2 \leq P_{\max}, \, \forall k \tag{28b}$$

$$\|\mathbf{F}_k\|_F^{-2} \leq \frac{\beta}{N_r \sigma_n^2}, \, \forall k \tag{28c}$$

where the second term is weighted by $(1-\alpha)$ in (28a), and it represents the sensing performance loss. The constraint in (28c) indicates the sensing QoS requirement with a threshold β [26]. This tradeoff optimization problem corresponds to the one formulated in $\mathbf{P1.1}$ with the shared antenna structure and omnidirectional beampattern (denoted as the "**shared-omni**" scheme). For the other combinations of schemes, in terms of separated antenna structure with omnidirectional beampattern (denoted as "**separated-omni**" scheme), shared antenna structure with directional beampattern (denoted as "**shared-direction**" scheme), and separated antenna structure with directional beampattern (denoted as "**separated-direction**" scheme), the tradeoff optimization problems can be represented, respectively, as

$$\mathbf{P2.2} \quad \min_{\mathbf{F},\mathbf{W},\bar{\mathbf{F}}} \alpha \boldsymbol{\mathcal{F}}_{2.1}\left(\mathbf{F}_k, \mathbf{W}, \bar{\mathbf{F}}_k\right) + (1-\alpha) \sum_{k=1}^{K} \|\bar{\mathbf{F}}_k - \bar{\mathbf{F}}_k^*\|_F^2 \tag{29a}$$

$$s.t. \quad \|\mathbf{F}_k\|_F^2 + \|\bar{\mathbf{F}}_k\|_F^2 \leq P_{\max}, \, \forall k \tag{29b}$$

$$\|\bar{\mathbf{F}}_k\|_F^{-2} \leq \frac{\beta}{N_r \sigma_n^2}, \, \forall k \tag{29c}$$

[5]The detailed procedures are not presented again for the sake of brevity, as they follow the same steps.

$$\mathcal{L}_{P2.1}(\mathbf{F}_k,\mathbf{W},\lambda_k,\rho)=\boldsymbol{\mathcal{F}}_{2.1}\left(\mathbf{F}_k,\mathbf{W}\right)+\sum_{k=1}^{K}\lambda_k\mathbf{Tr}\left(\mathbf{F}_k\mathbf{F}_k^H-\mathbf{R}_k\right)+\frac{\rho}{2}\sum_{k=1}^{K}\|\mathbf{F}_k\mathbf{F}_k^H-\mathbf{R}_k\|_F^2\ . \tag{26}$$

$$\begin{aligned}\mathcal{L}_{P2.2}(\mathbf{F}_k,\mathbf{W},\bar{\mathbf{F}}_k,\lambda_k^1,\lambda_k^2,\rho_1,\rho_2)=&\boldsymbol{\mathcal{F}}_{2.2}\left(\mathbf{F}_k,\mathbf{W},\bar{\mathbf{F}}_k\right)+\sum_{k=1}^{K}\lambda_k^1\mathbf{Tr}\left(\bar{\mathbf{F}}_k\bar{\mathbf{F}}_k^H-\mathbf{R}_k\right)+\frac{\rho_1}{2}\sum_{k=1}^{K}\|\bar{\mathbf{F}}_k\bar{\mathbf{F}}_k^H-\mathbf{R}_k\|_F^2\\&+\sum_{k=1}^{K}\lambda_k^2\left(\|\mathbf{F}_k\|_F^2+\|\bar{\mathbf{F}}_k\|_F^2-P_{\max}\right)+\frac{\rho_2}{2}\sum_{k=1}^{K}\left(\|\mathbf{F}_k\|_F^2+\|\bar{\mathbf{F}}_k\|_F^2-P_{\max}\right)^2\ .\end{aligned} \tag{27}$$

$$\begin{aligned}\mathcal{L}_{P4.2}(\mathbf{F}_k,\mathbf{W},\bar{\mathbf{F}}_k,\lambda_k^1,\lambda_k^2,\rho_1,\rho_2)=&\alpha\boldsymbol{\mathcal{F}}_{4.1}\left(\mathbf{F}_k,\mathbf{W},\bar{\mathbf{F}}_k\right)+(1-\alpha)\sum_{k=1}^{K}\|\bar{\mathbf{F}}_k-\bar{\mathbf{F}}_k^*\|_F^2+\sum_{k=1}^{K}\lambda_1\left(\|\mathbf{F}_k\|_F^2+\|\bar{\mathbf{F}}_k\|_F^2-P_{\max}\right)\\&+\frac{\rho_1}{2}\sum_{k=1}^{K}\left(\|\mathbf{F}_k\|_F^2+\|\bar{\mathbf{F}}_k\|_F^2-P_{\max}\right)^2+\sum_{k=1}^{K}\lambda_k^2\left(\|\mathbf{F}_k\|_F^{-2}-\frac{\beta}{N_r\sigma_n^2}\right)\\&+\frac{\rho_2}{2}\sum_{k=1}^{K}\left(\|\mathbf{F}_k\|_F^{-2}-\frac{\beta}{N_r\sigma_n^2}\right)^2\ .\end{aligned} \tag{32}$$

and

$$\mathbf{P3.2}\quad\min_{\mathbf{F},\mathbf{W}}\ \alpha\boldsymbol{\mathcal{F}}_{3.1}\left(\mathbf{F}_k,\mathbf{W}\right)+(1-\alpha)\sum_{k=1}^{K}\|\mathbf{F}_k-\mathbf{F}_k^*\|_F^2 \tag{30a}$$

$$s.t.\quad\text{(28b) and (28c)} \tag{30b}$$

and

$$\mathbf{P4.2}\quad\min_{\mathbf{F},\mathbf{W},\bar{\mathbf{F}}}\ \alpha\boldsymbol{\mathcal{F}}_{4.1}\left(\mathbf{F}_k,\mathbf{W},\bar{\mathbf{F}}_k\right)+(1-\alpha)\sum_{k=1}^{K}\|\bar{\mathbf{F}}_k-\bar{\mathbf{F}}_k^*\|_F^2 \tag{31a}$$

$$s.t.\quad\text{(29b) and (29c)}\ . \tag{31b}$$

which are corresponding to the beampattern design schemes in problem $\mathbf{P2.1}$, $\mathbf{P3.1}$, and $\mathbf{P4.1}$, respectively.

B. Gradient Descent Augmented Lagrangian Method

Similar to the optimization problems $\mathbf{P1.1}$ to $\mathbf{P1.4}$, we use the proposed GDAL algorithm to derive the desired $\mathbf{F},\mathbf{W}$, and $\bar{\mathbf{F}}$. To demonstrate the procedures, we only select a more complex problem, i.e., problem $\mathbf{P4.2}$ for the scheme of "**separated-direction**", and show the detailed derivation only for this problem. The corresponding derivations for $\mathbf{P1.2}-\mathbf{P3.2}$ follow similar procedures, which are not covered here for the sake of brevity.

First, the augmented Lagrangian function is defined in (32) at the top of this page, taking into account the maximum transmit power $P_{\max}$ and their sensing QoS requirement β. Before updating the variables $\mathbf{F}_k^l,\mathbf{W}^l$ and $\bar{\mathbf{F}}_k^l$ at the l-th iteration using the gradient descent method, the corresponding gradients are computed as

$$\begin{aligned}\nabla_{\mathbf{W}}\mathcal{L}_{P4.2}=&\,2\alpha\sum_{k=1}^{K}\mathbf{H}_k\mathbf{F}_k\left(\mathbf{W}^H\mathbf{H}_k\mathbf{F}_k-\mathbf{A}\right)\\&+2\alpha\left[\sum_{k=1}^{K}\bar{\mathbf{H}}_k^H\bar{\mathbf{F}}_k\mathbf{W}^H\bar{\mathbf{H}}_k\bar{\mathbf{F}}_k+2\sigma_n^2\mathbf{W}\right]\end{aligned} \tag{33}$$

$$\begin{aligned}\nabla_{\mathbf{F}_k}\mathcal{L}_{P4.2}=&\,2\alpha\mathbf{H}_k^H\mathbf{W}\left(\mathbf{W}^H\mathbf{H}_k\mathbf{F}_k-\mathbf{A}\right)+2\lambda_k^1\mathbf{F}_k\\&+2\rho_1\left(\|\mathbf{F}_k\|_F^2+\|\bar{\mathbf{F}}_k\|_F^2-P_{\max}\right)\end{aligned} \tag{34}$$

$$\begin{aligned}\nabla_{\bar{\mathbf{F}}_k}\mathcal{L}_{P4.2}=&\,2\alpha\bar{\mathbf{H}}_k^H\mathbf{W}\mathbf{W}^H\bar{\mathbf{H}}_k\bar{\mathbf{F}}_k+2(1-\alpha)\left(\bar{\mathbf{F}}_k-\bar{\mathbf{F}}_k^*\right)\\&+2\rho_1\left(\|\mathbf{F}_k\|_F^2+\|\bar{\mathbf{F}}_k\|_F^2-P_{\max}\right)\bar{\mathbf{F}}_k\\&-2\rho_2\left(\|\mathbf{F}_k\|_F^{-2}-\frac{\beta}{N_r\sigma_n^2}\right)\frac{\bar{\mathbf{F}}_k}{\|\bar{\mathbf{F}}_k\|_F^4}\\&+2\lambda_k^1\bar{\mathbf{F}}_k-2\lambda_k^2\frac{\bar{\mathbf{F}}_k}{\|\bar{\mathbf{F}}_k\|_F^4}\ .\end{aligned} \tag{35}$$

Then these variables are updated according to the updating rules defined in (17) - (19). Note that we also implement the AdaGrad method to adaptively updating the step sizes $\boldsymbol{\Phi}_{\mathbf{W}}$, $\boldsymbol{\Phi}_{\mathbf{F}_k}$, and $\boldsymbol{\Phi}_{\bar{\mathbf{F}}_k}$ for fast convergence. The Lagrange multipliers λ_k^1 and λ_k^2 are sequentially updated as

$$(\lambda_k^1)^{l+1}=(\lambda_k^1)^l+\rho_1^l\left(\|\mathbf{F}_k^{l+1}\|_F^2+\|\bar{\mathbf{F}}_k^{l+1}\|_F^2-P_{\max}\right) \tag{36}$$

$$(\lambda_k^2)^{l+1}=(\lambda_k^2)^l+\rho_2^l\left(\|\bar{\mathbf{F}}_k^{l+1}\|_F^{-2}-\frac{\beta}{N_r\sigma_n^2}\right)\ . \tag{37}$$

Corresponding updates of ρ_1 and ρ_2 follow the rule specified in (22). The overall algorithm stops once the bias of the value of Lagrangian function is not greater than the tolerance ϵ or the maximum number of iterations L is reached. Finally, we obtain $\mathbf{F}_k,\mathbf{W}$ and $\bar{\mathbf{F}}_k$ for sensing and AirComp under the constraints. The detailed derivation procedures are summarized in **Algorithm 2**.

Algorithm 2: GDAL Algorithm for Problem $\mathbf{P4.2}$

Input: Initialize $\mathbf{F}_k^0$, $\mathbf{W}^0$, $\bar{\mathbf{F}}_k^0$, λ_1^0, λ_2^0, ρ_1^0, ρ_2^0, $\mathbf{\Phi}_{\mathbf{F}_k}^0$, $\mathbf{\Phi}_{\mathbf{W}}^0$, $\mathbf{\Phi}_{\bar{\mathbf{F}}_k}^0$, tolerance ϵ, and maximum number of iterations L.

Output: Optimal $\mathbf{F}$, $\mathbf{W}$ and $\bar{\mathbf{F}}$

$l \leftarrow 0$;
while $l < L$ **do**
  Sequentially update the parameters:
  Compute the Lagrangian function value in (32);
  Compute gradients of $\nabla_{\mathbf{W}}\mathcal{L}_{P4.2}$, $\nabla_{\mathbf{F}_k}\mathcal{L}_{P4.2}$ and $\nabla_{\bar{\mathbf{F}}_k}\mathcal{L}_{P4.2}$ according to (33) - (35);
  Update $\mathbf{F}_k^{l+1}$, $\mathbf{W}^{l+1}$ and $\bar{\mathbf{F}}_k^{l+1}$ according to (17) - (19) ;
  Update Lagrange multipliers $(\lambda_k^1)^{l+1}$ and $(\lambda_k^2)^{l+1}$ in (36) - (37) ;
  Update penalty parameter: ρ_1^{l+1} and ρ_2^{l+1} according to the rule defined in (22) ;
  Check convergence criteria:
  if *convergence criteria met* **then**
    Output $\mathbf{F}$, $\mathbf{W}$ and $\bar{\mathbf{F}}$;
    break ;
  $l \leftarrow l + 1$;

V. Numerical Simulation

For comprehensive comparisons among the different combinations of antenna structures and beampattern types, the performance evaluation using our proposed algorithms is presented in this section. We assume that the AP has $N_A = 32$ antenna elements, and each robot has a total of $N_R = 24$ antenna elements. In the shared antenna structure setup, $N_t = N_r = 12$ for signal transmission and reception. For a fair comparison, we use the same number of antenna elements at each robot in the separated antenna structure setup, e.g., $N_s = N_c = 8$ for sensing and communication, and $N_r = 8$ for signal reception at the robot. For the IoRT scenario depicted in Fig. 1, the link condition between each robot and AP is modeled as follows: the link is assumed to be blocked with a probability p_b, and pathloss is calculated following the 3GPP [29]. We assume that the robot-AP link condition is either in LoS or Non-LoS (NLoS) with a dominant single path propagation, i.e., $M = 1$. However, we can extend it to any integer M according to the practical channel conditions to support the case of $M > 1$ AirComp functions. Furthermore, we use the abbreviation terms "**shared-omni**", "**shared-direction**", "**separated-omni**", and "**separated-direction**" to distinguish between different antenna and beampattern setups. The performance tradeoff between AirComp and sensing is weighted by a factor $\alpha = 0.5$ if no other specifications are given.

Fig. 2 illustrates the AirComp MSE under different maximum transmit power budgets. The AirComp MSE increases with the maximum power $P_{\max}$. Moreover, the MSE is in the range of approximately 10^{-7} to 10^{-5}. Those phenomena are due to the pathloss, which results in a low received power level. It is meaningful for practical deployment, which is different from the case of simple Gaussian channel modeling

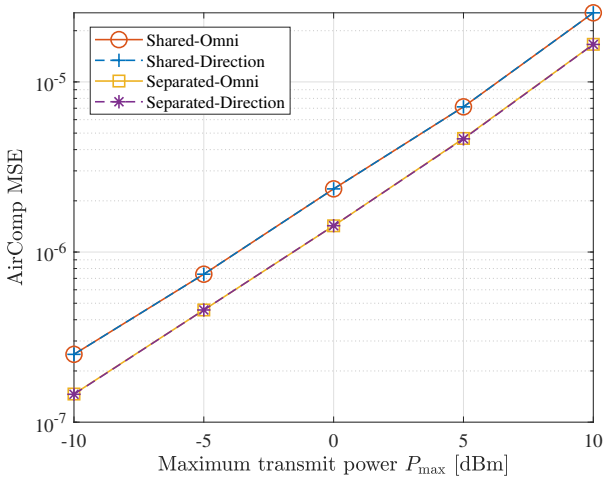

Fig. 2: AirComp MSE under different levels of power constraint: $K = 10, p_b = 0$.

with zero mean and unit variance, as considered in [7], [26]. It is also interesting to observe that beampattern types (omnidirectional and directional) almost have no effect on the AirComp MSE for the given antenna structure (shared or separated). This is because the AP itself can realize a variable beamwidth to cover all the robots within its sector area for uplink aggregated signal reception [27]. In such a case, the optimal beamforming combiner at the AP can be guaranteed. Moreover, one of our objectives is to minimize the AirComp MSE so that the expected beamforming precoder at each robot can also be ensured compared to the optimal one using our algorithm. It is observed that a lower AirComp MSE was achieved in Fig. 2 for the separated antenna structure compared to the shared one. This verifies that the separated antenna array for communication and sensing achieves a higher degree of freedom for beam steering compared to the dual-functional beamforming in a shared antenna structure.

If the number of robots increases, it is challenging to design an aggregation beamforming combiner at the AP to receive the uplink AirComp signals within its coverage. This is because the larger the number of robots randomly distributed within the AP's coverage area, the larger the beamwidth is needed for the AP to cover all the robots, which results in a lower beamforming gain such that a larger MSE is obtained, as shown in Fig. 3(a) in the top of the next page. In addition, the separated antenna structure has a lower AirComp MSE than the shared antenna structure, which is similar to the results shown in Fig. 2. This is because it has a higher degree of freedom for spatial beam steering. Moreover, the beampattern has almost no effect on the MSE for a given antenna structure. Fig. 3(b) shows that the sensing MSE maintains a relatively stable level for given setups though a slightly decrease for the separated antenna configurations. This is because the sensing precoder is derived for each robot separately so that the sensing performance can always be guaranteed, and it is almost not affected by the number of robots. The increased number of robots only has significant effects on aggregation beamforming

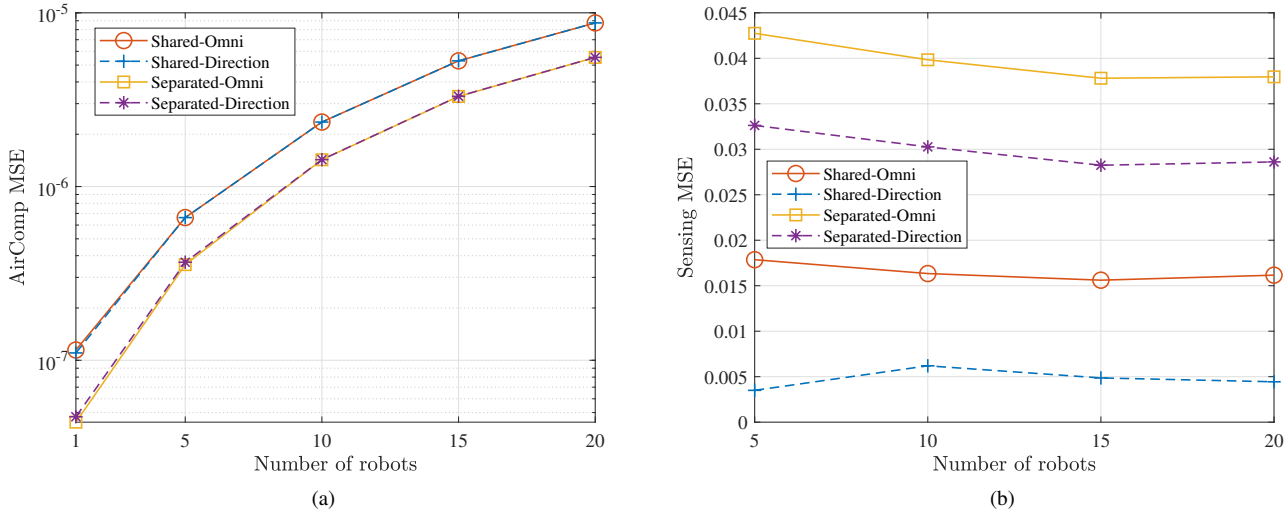

Fig. 3: MSE performance affected by the number of robots ($P_{\max} = 0$ dBm, $p_b = 0$): (a) AirComp MSE, (b) Sensing MSE.

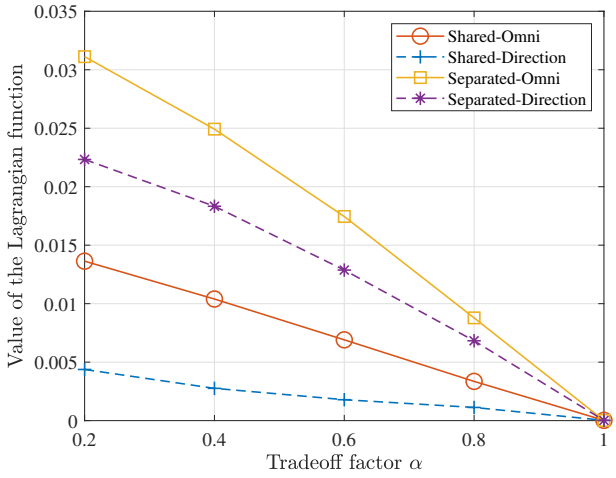

Fig. 4: Tradeoff factor effects on the value of the Lagrangian function: $K = 10, P_{\max} = 10\,\text{dBm}, p_b = 0$.

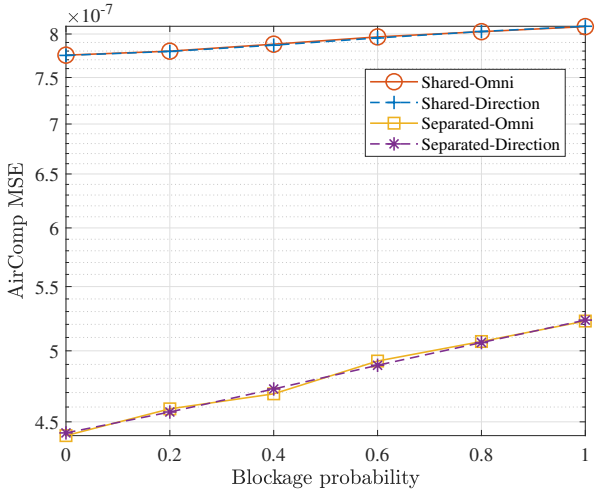

Fig. 5: Blockage effects on the AirComp MSE: $K = 5, P_{\max} = 0\,\text{dBm}$.

design at the AP, which reflects in the AirComp performance, as illustrated in Fig. 3(a). Furthermore, it is observed that the directional beampattern achieves a lower sensing MSE for a given antenna structure setup. The separated antenna structure configuration yields a higher sensing MSE than the shared antenna setup because the two separate antenna arrays shared the total transmit power budget for sensing and communication, as detailed in (3) and (8).

In Fig. 4, we assess the impact of the tradeoff factor α on the value of the Lagrangian function. It is evident that the value of the Lagrangian function exhibits a notable decrease with increasing α. This is attributed to the augmented weight on the AirComp MSE as α increases, which leads to a diminished Lagrangian function value. This is especially true when the robot-AP link pathloss is taken into account.

We also evaluate the blockage probability effects on the AirComp MSE in Fig. 5. The blockage probability has remarkable effects on the scheme of the separated antenna structure compared to the shared antenna setup. This is due to the fact that the separated antenna configuration has a power division into two antenna arrays for sensing and AirComp, respectively. This causes uplink AirComp to have low transmit power. Furthermore, the AirComp link between each robot and the AP is not fully blocked even if a blockage event occurs [29], [41]. As a consequence, the AirComp MSE for the shared antenna setup does not show a remarkably sharp increase with the blockage probability.

VI. Conclusion

In this paper, a comprehensive investigation of the antenna structures and beampatterns for the ISCC system in an IoRT scenario has been presented. There are four MSE minimization optimization problems formulated among different setups in terms of "**shared-omni**", "**shared-direction**",

"**separated-omni**", and "**separated-direction**" that involve a weighted factor to tradeoff the performance between AirComp and sensing. To efficiently solve the formulated non-convex optimization problems, we have designed the GDAL algorithm with an adaptive adjustment of the step sizes in the variable updates. The simulations have shown that the separated antenna structure achieves a lower AirComp MSE than the shared antenna setups because it has higher degrees of freedom for beam steering. Moreover, the beampattern has almost no effect on the AirComp MSE for a given antenna structure setup at the robots. The relatively stable sensing performance can be guaranteed for a given setup even if the number of robots increases, however, choosing an increased number of robots for localization accuracy improvement increases the complexity of the ISCC system, especially for resource scheduling. In practical IoRT scenarios, we must strike a balance between complexity and target localization accuracy. Moreover, it is more sensitive to the blockage for the separated antenna setups due to the power split for sensing and communication, which results in a remarkable increase in AirComp MSE as the blockage probability increases. These findings have meaningful guidelines for practical IoRT networks. For example, we can implement more efficient resource allocation schemes for wireless link scheduling by using the ISCC framework for target localization and blockage detection. This will improve the end-to-end link quality in deterministic wireless networking.

REFERENCES

[1] D. C. Nguyen, M. Ding, P. N. Pathirana, A. Seneviratne, J. Li, D. Niyato, O. Dobre, and H. V. Poor, "6G Internet of Things: A comprehensive survey," *IEEE Internet of Things Journal*, vol. 9, no. 1, pp. 359–383, 2021.

[2] Y. Liu, X. Liu, X. Gao, X. Mu, X. Zhou, O. A. Dobre, and H. V. Poor, "Robotic communications for 5G and beyond: Challenges and research opportunities," *IEEE Communications Magazine*, vol. 59, no. 10, pp. 92–98, 2021.

[3] F. Liu, Y. Cui, C. Masouros, J. Xu, T. X. Han, Y. C. Eldar, and S. Buzzi, "Integrated sensing and communications: Toward dual-functional wireless networks for 6G and beyond," *IEEE Journal on Selected Areas in Communications*, vol. 40, no. 6, pp. 1728–1767, 2022.

[4] Y. Cui, F. Liu, X. Jing, and J. Mu, "Integrating sensing and communications for ubiquitous IoT: Applications, trends, and challenges," *IEEE Network*, vol. 35, no. 5, pp. 158–167, 2021.

[5] C. Wang, B. Jia, H. Yu, X. Li, X. Wang, and T. Taleb, "Deep reinforcement learning for dependency-aware microservice deployment in edge computing," in *GLOBECOM 2022-2022 IEEE Global Communications Conference*. IEEE, 2022, pp. 5141–5146.

[6] S. H. Alsamhi, O. Ma, and M. S. Ansari, "Survey on artificial intelligence based techniques for emerging robotic communication," *Telecommunication Systems*, vol. 72, pp. 483–503, 2019.

[7] X. Li, F. Liu, Z. Zhou, G. Zhu, S. Wang, K. Huang, and Y. Gong, "Integrated sensing, communication, and computation over-the-air: MIMO beamforming design," *IEEE Transactions on Wireless Communications*, vol. 22, no. 8, pp. 5383–5398, 2023.

[8] A. Liu, Z. Huang, M. Li, Y. Wan, W. Li, T. X. Han, C. Liu, R. Du, D. K. P. Tan, J. Lu *et al.*, "A survey on fundamental limits of integrated sensing and communication," *IEEE Communications Surveys & Tutorials*, vol. 24, no. 2, pp. 994–1034, 2022.

[9] F. Liu, L. Zhou, C. Masouros, A. Li, W. Luo, and A. Petropulu, "Toward dual-functional radar-communication systems: Optimal waveform design," *IEEE Transactions on Signal Processing*, vol. 66, no. 16, pp. 4264–4279, 2018.

[10] Z. Xiao and Y. Zeng, "Full-duplex integrated sensing and communication: Waveform design and performance analysis," in *Proceeding IEEE 13th International Conference on Wireless Communications and Signal Processing (WCSP)*, Changsha, China, October 2021, pp. 1–5.

[11] Z. Wei, J. Piao, X. Yuan, H. Wu, J. A. Zhang, Z. Feng, L. Wang, and P. Zhang, "Waveform design for MIMO-OFDM integrated sensing and communication system: An information theoretical approach," *IEEE Transactions on Communications*, vol. 72, no. 1, pp. 496–509, 2023.

[12] Z. Xing, R. Wang, and X. Yuan, "Joint active and passive beamforming design for reconfigurable intelligent surface enabled integrated sensing and communication," *IEEE Transactions on Communications*, vol. 71, no. 4, pp. 2457–2474, 2023.

[13] X. Liu, Y. Liu, Z. Liu, and T. S. Durrani, "Fair integrated sensing and communication for multi-UAV enabled internet of things: Joint 3D trajectory and resource optimization," *IEEE Internet of Things Journal*, 2023.

[14] X. Li, Y. Gong, K. Huang, and Z. Niu, "Over-the-air integrated sensing, communication, and computation in IoT networks," *IEEE Wireless Communications*, vol. 30, no. 1, pp. 32–38, 2023.

[15] P. Porambage, J. Okwuibe, M. Liyanage, M. Ylianttila, and T. Taleb, "Survey on multi-access edge computing for internet of things realization," *IEEE Communications Surveys & Tutorials*, vol. 20, no. 4, pp. 2961–2991, 2018.

[16] T. Taleb, K. Samdanis, B. Mada, H. Flinck, S. Dutta, and D. Sabella, "On multi-access edge computing: A survey of the emerging 5G network edge cloud architecture and orchestration," *IEEE Communications Surveys & Tutorials*, vol. 19, no. 3, pp. 1657–1681, 2017.

[17] Y. Chen, N. Zhang, Y. Zhang, and X. Chen, "Dynamic computation offloading in edge computing for internet of things," *IEEE Internet of Things Journal*, vol. 6, no. 3, pp. 4242–4251, 2018.

[18] Q. Wang, R. Q. Hu, Y. Qian *et al.*, "Hierarchical energy-efficient mobile-edge computing in IoT networks," *IEEE Internet of Things Journal*, vol. 7, no. 12, pp. 11 626–11 639, 2020.

[19] Z. Zhuang, D. Wen, Y. Shi, G. Zhu, S. Wu, and D. Niyato, "Integrated sensing-communication-computation for over-the-air edge AI inference," *IEEE Transactions on Wireless Communications*, vol. 23, no. 4, pp. 3205–3220, 2023.

[20] Q. Qi, X. Chen, C. Zhong, and Z. Zhang, "Integrated sensing, computation and communication in B5G cellular internet of things," *IEEE Transactions on Wireless Communications*, vol. 20, no. 1, pp. 332–344, 2020.

[21] G. Zhu, J. Xu, K. Huang, and S. Cui, "Over-the-air computing for wireless data aggregation in massive IoT," *IEEE Wireless Communications*, vol. 28, no. 4, pp. 57–65, 2021.

[22] W. Fang, Y. Jiang, Y. Shi, Y. Zhou, W. Chen, and K. B. Letaief, "Over-the-air computation via reconfigurable intelligent surface," *IEEE Transactions on Communications*, vol. 69, no. 12, pp. 8612–8626, 2021.

[23] A. Şahin and R. Yang, "A survey on over-the-air computation," *IEEE Communications Surveys & Tutorials*, vol. 25, no. 3, pp. 1877–1908, 2023.

[24] Q. Qi, X. Chen, A. Khalili, C. Zhong, Z. Zhang, and D. W. K. Ng, "Integrating sensing, computing, and communication in 6G wireless networks: Design and optimization," *IEEE Transactions on Communications*, vol. 70, no. 9, pp. 6212–6227, 2022.

[25] Y. Zuo, M. Yue, H. Yang, L. Wu, and X. Yuan, "Integrating communication, sensing and computing in satellite internet of things: Challenges and opportunities," *IEEE Wireless Communications*, vol. 31, no. 3, pp. 332–338, 2024.

[26] S. Wang, Y. Gong, X. Li, and Q. Li, "Integrated sensing, communication and computation over-the-air: Beampattern design for wireless sensor networks," *IEEE Internet of Things Journal*, vol. 11, no. 6, pp. 9681–9692, 2023.

[27] K. Dong, S. Mura, M. Mizmizi, D. Tagliaferri, and U. Spagnolini, "Advanced tri-sectoral multi-user millimeter-wave smart repeater," in *Proceeding IEEE International Mediterranean Conference on Communications and Networking (MeditCom)*, Dubrovnik, Croatia, September 2023, pp. 205–210.

[28] Z. Liu, Y. Liu, and X. Chu, "Reconfigurable intelligent surface-assisted indoor millimeter-wave communications for mobile robots," *IEEE Internet of Things Journal*, vol. 11, no. 1, pp. 1548–1557, 2023.

[29] 3rd Generation Partnership Project (3GPP), "Study on channel model for frequencies from 0.5 to 100 GHz," vol. TR 38.901, Tech. Rep., December 2019.

[30] A. Alkhateeb, O. El Ayach, G. Leus, and R. W. Heath, "Channel estimation and hybrid precoding for millimeter wave cellular systems," *IEEE Journal of Selected Topics in Signal Processing*, vol. 8, no. 5, pp. 831–846, 2014.

[31] A. Abdallah, A. Celik, M. M. Mansour, and A. M. Eltawil, "RIS-aided mmwave MIMO channel estimation using deep learning and compressive sensing," *IEEE Transactions on Wireless Communications*, vol. 22, no. 5, pp. 3503–3521, 2022.

[32] A. M. Elbir, K. V. Mishra, S. A. Vorobyov, and R. W. Heath, "Twenty-five years of advances in beamforming: From convex and nonconvex optimization to learning techniques," *IEEE Signal Processing Magazine*, vol. 40, no. 4, pp. 118–131, 2023.

[33] Y. You, W. Zhao, L. Zhang, X. You, and C. Zhang, "Beam pattern and reflection pattern design for channel estimation in RIS-assisted mmwave mimo systems," *IEEE Transactions on Vehicular Technology*, vol. 73, no. 4, pp. 5915–5919, 2023.

[34] D. P. Kingma and J. Ba, "Adam: A method for stochastic optimization," in *Proceeding 3rd International Conference on Learning Representations (ICLR)*, San Diego, CA, USA, May 2015.

[35] L. Luo, Y. Xiong, Y. Liu, and X. Sun, "Adaptive gradient methods with dynamic bound of learning rate," in *Proceeding 3rd International Conference on Learning Representations (ICLR)*, New Orleans, LA, USA, May 2019.

[36] J. Duchi, E. Hazan, and Y. Singer, "Adaptive subgradient methods for online learning and stochastic optimization." *Journal of Machine Learning Research*, vol. 12, no. 7, pp. 2121–2159, 2011.

[37] A. Khabbazibasmenj, A. Hassanien, S. A. Vorobyov, and M. W. Morency, "Efficient transmit beamspace design for search-free based doa estimation in MIMO radar," *IEEE Transactions on Signal Processing*, vol. 62, no. 6, pp. 1490–1500, 2014.

[38] A. Hassanien and S. A. Vorobyov, "Phased-MIMO radar: A tradeoff between phased-array and MIMO radars," *IEEE Transactions on Signal Processing*, vol. 58, no. 6, pp. 3137–3151, 2010.

[39] M. Grant and S. Boyd, "CVX: Matlab software for disciplined convex programming, version 2.1," 2014.

[40] M. C. Grant and S. P. Boyd, "Graph implementations for nonsmooth convex programs," in *Recent Advances in Learning and Control*. Springer, 2008, pp. 95–110.

[41] K. Dong, M. Mizmizi, D. Tagliaferri, and U. Spagnolini, "Vehicular blockage modelling and performance analysis for mmwave V2V communications," in *Proceeding IEEE International Conference on Communications*, Seoul, South Korea, May 2022, pp. 3604–3609.